




Semiconducting Plant Extracts of *Cucurbita Pepo L.* Seeds for Facile, Inexpensive, Fully Solution-Processed, Transparent Photodetector Fabrication

Muzeyyen Savas¹, Beyza Bozkurt², Dilber Akcan³, Ruby Phul¹ , Talha Erdem^{1,*} , Zeliha Soran-Erdem^{3,4,*} 

¹Department of Electrical-Electronics Engineering, Abdullah Gül University, Kayseri 38080 Türkiye

²Department of Molecular Biology and Genetics, Abdullah Gül University, Kayseri 38080 Türkiye

³Bioengineering Program, Graduate School of Engineering and Science, Abdullah Gül University, Kayseri 38080 Türkiye

⁴Department of Engineering Sciences, Abdullah Gül University, Kayseri 38080 Türkiye

(Alınış / Received: 26.04.2024, Kabul / Accepted: 03.07.2024, Online Yayınlanma / Published Online: 30.08.2024)

Keywords

Plant extract,
Pumpkin seed,
Cucurbita pepo L.,
Photodetectors.

Abstract: Solution-processable materials attract significant interest in the development of high-efficiency, cost-effective optoelectronic devices. However, widely used high-performance materials often suffer from high toxicity, low biocompatibility, and synthesis procedures hazardous to human health and the environment. As cost-effective, sustainable alternatives to the conventional solution-processed semiconductors, here we evaluate the potential of plant extracts. Within this framework, here we present photodetectors employing the extract of *Cucurbita pepo L.* (pumpkin) seeds. The extracted material exhibits a strong absorption peak in the UV region (~280 nm) and a weaker absorption band between 400-450 nm. Its fluorescence spectrum covers the blue-green region of the spectrum and possesses sharp and dominant peaks at 650 nm and 730 nm. For photodetector fabrication, we drop-cast the extract acting as the active material between two electric contacts formed by treating a conductive film of silver nanowires and zinc oxide nanoparticles using a surgical blade. The resulting device demonstrates a maximum responsivity of ~1.61 mA/W at 5 V bias voltage. Being fully solution-processed, transparent photodetectors, this proof-of-concept device employing plant extracts showcases a new material system in active optoelectronic devices as sustainable, inexpensive, and easy-to-handle alternatives to their conventional counterparts.

Kolay, Ucuz, Tamamen Çözeltiyle İşlenmiş ve Şeffaf Fotodetektör Üretimi için *Cucurbita Pepo L.* Tohumlarının Yarı İletken Bitki Özütleri

Anahtar Kelimeler

Bitki ekstraktı,
Balkabağı çekirdeği,
Cucurbita pepo L.,
Fotodetektör.

Öz: Çözeltide işlenebilen malzemeler, yüksek verimli ve uygun maliyetli optoelektronik cihazların geliştirilmesinde büyük ilgi görmektedir. Bununla birlikte, yaygın olarak kullanılan yüksek performanslı malzemeler sıklıkla yüksek toksisiteye, düşük biyoyoumluluğa ve insan sağlığına ve çevreye zararlı sentez prosedürlerine sahiptir. Geleneksel, çözeltiyle işlenmiş yarı iletkenlere uygun maliyetli ve sürdürülebilir alternatifler olarak, sunulan çalışmada bitki ekstraktlarının potansiyeli araştırılmaktadır. Bu çerçevede, burada *Cucurbita pepo L.* (balkabağı) çekirdeği ekstraktı içeren fotodetektörler sunulmaktadır. Balkabağı çekirdeğinden elde edilen özütümüz, UV bölgesinde (~280 nm) güçlü bir soğurma gösterirken, 400-450 nm arasında daha zayıf bir soğurma bandına sahiptir. Özütün floresans spektrumu incelendiğinde, ışımının mavi-yeşil spektrum bölgesinde özellikle de 650 nm ve 730 nm'de keskin ve baskın tepe noktalarına sahip olduğu görülmektedir. Fotodetektör üretimi için, gümüş nanotellerden ve çinko oksit

nanopartiküllerinden oluşan iletken bir filmin cerrahi bir bıçak kullanılarak işlenmesiyle iki elektrik kontağı oluşturulmuş, daha sonra bu iki kontak arasına aktif malzeme görevi gören ekstrakt damlatılmıştır. Ortaya çıkan cihaz, 5 V öngerilim voltajında $\sim 1,61$ mA/W'lik maksimum yanıt vermiştir. Bu çalışmada ürettiğimiz tamamen çözeltiyle işlenmiş, şeffaf ve bitki özü içeren konsept ispatı fotodetektör cihazı, aktif optoelektronik cihazlarda geleneksel muadillerine göre sürdürülebilir, ucuz ve kullanımı kolay alternatif yeni bir malzeme sistemi olarak gelecek çalışmalara ışık tutacaktır.

*İlgili Yazar, email: zsoran@gmail.com

1. Introduction

Plants offer a vast array of bioactive compounds, such as flavonoids, alkaloids, carotenoids, saponins, and polyphenols, which are widely utilized in the food, pharmaceutical, and cosmetic industries for their antioxidant and antimicrobial properties [1], [2], [3], [4]. Another important property of some plant species is autofluorescence which stands for the ability of the plants to emit visible light upon excitation at a suitable wavelength [5]. Autofluorescence occurs owing to the presence of fluorescent, semiconducting pigments that are densely produced in plant tissues [6]. Considering their semiconducting and eco-friendly nature, plant-based compounds are promising alternatives to synthetic, non-biocompatible, and carcinogenic semiconductors. Owing to these strengths, such natural semiconductors promise improved eco-friendliness and biodegradability of optoelectronic devices. Nevertheless, despite their potential, these natural semiconductors currently remain underutilized in optoelectronic technologies.

As part of our attempts towards achieving more sustainable optoelectronic technologies, here we study pumpkin seed extracts. Pumpkins are members of the *Cucurbitaceae* family and the *Cucurbita* genus of gourd squashes, and they are commonly grown worldwide for both decorative and culinary applications [7]. Approximately 44% of their seeds consist of oil, with linoleic acid being the predominant fatty acid (42–59%) and oleic acid comprising 25% [7], [8]. Thanks to their high nutritional value and rich composition of essential fatty acids, vitamins, and minerals, pumpkin seed oil (PSO) has great potential for use as a functional food and edible oil [9]. Their fluorescence characteristics have also been studied in literature [7], [10]. For example, Borthakur and Barua [7] studied the relation between the fluorescence changes of *Cucurbita pepo L.* and the ripening stage of the fruit. According to their findings, the content of fluorophores in the fruit changes during growth, leading to variations in the fluorescence spectra of pumpkin seed extracts. However, to the best of our knowledge, the use of pumpkin seed extracts in optoelectronic devices remains unexplored.

Optoelectronic devices heavily rely on inorganic materials including silicon, germanium, or gallium-containing compounds (e.g., GaAsP, AlInGaN) that are expensive and environmentally hazardous to produce [11], [12]. Finding alternatives to these conventional materials has become crucial for making optoelectronics industry more sustainable. Solution-processed materials step forward as an important class of materials that eliminate the need for costly and energy-consuming growth methods. Perovskites [13], colloidal quantum dots (CQDs) [14], semiconducting organic molecules [15], and polymers [16] have been widely employed as active materials in these devices. However, the Cd content in the CQDs, the Pb content in the perovskites, and the toxic solvents such as dimethylformamide and dimethyl sulfoxide used during the synthesis of polymers substantially decrease the environmental compatibility of these solution-processed semiconducting materials. Therefore, environmentally-friendly alternatives are sought for achieving sustainable optoelectronics. At this point, semiconductors obtained from natural sources step forward. Since plant extracts like the pumpkin seed extract we employ in this work have a natural origin and are considered biodegradable, they are decomposable by natural processes without causing long-term environmental harm.

To make optoelectronic device fabrication more sustainable, optimization of materials is not enough. Instead, the whole fabrication system needs to comply with the principles of sustainable production. With this motivation, our team has recently presented a low-cost fabrication method for fully solution-processed, colloidal quantum dot (CQD) photodetectors [17], [18]. While the active material in these devices were Cd-based colloidal quantum dots, we employed a surgical blade to define the electrical contacts instead of using conventional lithography techniques [19], [20], [21], making the fabrication significantly cheaper and energy-efficient.

In this study, we further improve the sustainability of solution-processed photodetectors by introducing plant extracts for the first time as the active material of a photodetector instead of conventional environmentally harmful substances. To achieve this, we extracted the seeds of *Cucurbita pepo L.* which can absorb light over a broad wavelength range and emit orange-red light at around 630 nm and utilized its extract as the active material

in our proof-of-concept photodetector. Similar to our previous work [17], [18], we formed electric contacts by opening a 30 μm wide gap on a conductive film made of silver nanowires and zinc oxide nanoparticles. Subsequently, we completed the device structure by drop-casting the extract of the seeds of *Cucurbita pepo L.* between the electric contacts. The resulting proof-of-concept device exhibited responsivities up to 1.61 mA/W proving that simple, sustainable photodetectors can be produced using plant extracts. Considering that this is the first example of a photodetector relying on plant extracts, we believe that there is a substantial room for performance improvements through material and device optimization. With further improvements, we conceive that plant extracts will find applications in photodetectors as environmentally friendly, cost-effective, solution-processed semiconductors.

2. Material and Method

2.1 Chemicals and materials

Pumpkin seeds (*Cucurbita pepo*), n-hexane ($\geq 96\%$, Merck), Whatman qualitative filter papers, Syringe Filters PTFE Membrane 0.22 μm pore size (ISOLAB USA). Polyvinylpyrrolidone (PVP, $M_w \approx 40000$, powder), silver nitrate (AgNO_3 , 99.0%), sodium chloride (NaCl , 99.5%), potassium bromide (KBr , 99.0%), ethylene glycol (EG, 99.0%), ethanol absolute ($\geq 99.9\%$, Isolab), acetone (EMSURE, Merck), methanol ($\geq 99.7\%$, Sigma-Aldrich). Zinc acetate dehydrate ($\text{ZnAc}_2 \cdot 2\text{H}_2\text{O}$, 99.999%), dimethyl sulfoxide (DMSO, Merck), tetramethylammonium hydroxide pentahydrate (TMAH, $\geq 97\%$, Sigma-Aldrich), ethanol absolute ($\geq 99.9\%$, Isolab), acetone (EMSURE, Merck), n-hexane ($\geq 96\%$, Merck). *Cucurbita pepo* seeds were collected from a local grocery store, and all other chemicals and reagents were purchased from Sigma-Aldrich unless otherwise stated and used without further purification.

2.2 Preparation of pumpkin seed extract

Prior to extraction, pumpkin seeds were dried, peeled, and then ground using a mortar. Subsequently, 5 g of the ground pumpkin seeds were mixed with 25 mL of hexane, and the extraction was carried out in a 50 ml round bottom flask at 60 $^\circ\text{C}$ with continuous stirring and refluxing with nitrogen for 2 hours. Afterwards, the extract was allowed to cool to room temperature (RT) and was cleaned in three steps. For this purpose, first, the extract was filtered using a Whatman paper, and then the solution was centrifuged at 10,000 rpm for 10 min twice. Finally, the supernatant was filtered using an ISOLAB PTFE hydrophobic syringe filter with a 0.22 μm pore size, and the extract was stored at 4 $^\circ\text{C}$ until they were used in experiments.

2.3 Synthesis of silver nanowires

Silver nanowires were prepared using a polyol process, presented by Kim *et al.*, with some modifications [22]. Initially, 1.6 g of PVP was added to 50 mL of EG in a two-necked flat-bottom flask and stirred at 450 rpm using a magnetic stirrer until PVP was completely dissolved in EG. The mixture was then heated to 170 $^\circ\text{C}$, and 0.05 g of NaCl , 0.025 g of KBr , and 0.7 g of AgNO_3 were added to the solution as soon as it reached 170 $^\circ\text{C}$ and conserved stirring. Next, the solution was kept at 170 $^\circ\text{C}$ for 3 h to allow the Ag nanowire growth reaction to take place and then was cooled down to room temperature by moving the flask into a water bath. To clean, the nanowire solution was centrifuged with methanol and acetone twice. The collected Ag NWs were finally dispersed in ethanol according to the desired concentration.

2.4 Synthesis of zinc oxide nanoparticles

ZnO nanoparticles were synthesized using the modified sol-gel method developed by Jin *et al.* [23] Two different solutions were prepared for the synthesis. For the first solution, 30 mL of dimethyl sulfoxide (DMSO) was used to dissolve 0.6585 g of zinc acetate dihydrate. The solution was then left to stir. Second, a tetramethylammonium hydroxide pentahydrate (TMAH) solution in ethanol was prepared (0.5 M, 10 mL). The TMAH solution was added to the zinc acetate dihydrate solution at a rate of 8 mL/min while stirring. Then, without pausing the mixing process, the solutions were allowed to react for an hour under ambient conditions. After the reaction was completed, the resulting solution was equally divided into three 50 mL falcon tubes, which were then filled with acetone [24], and the content was centrifuged for 5 minutes at 5000 rpm. The precipitate was preserved once this process was finished, and the supernatant was poured out. Each falcon tube was then filled with 1 mL of ethanol and sonicated in a cold sonicator for 10 minutes. Subsequently, each 1 mL solution was mixed with 24 mL of acetone and 25 mL of hexane, and the solutions were centrifuged at 5000 rpm for 10 min. Similarly, the liquid portion of the falcon had been drained after the centrifugation process, and 1.5 mL of ethanol was added. Before further use, they were sonicated for 15 minutes in a cooled sonicator.

2.5 Fabrication of the photodetector

To prepare photodetectors with PSE, Ag NW and ZnO NP loadings were fixed at 2 mg mL^{-1} and 5 mg mL^{-1} , respectively. The fabrication process starts with cleaning 2.5x2.5 cm^2 glass substrates. The substrates were initially cleaned in an ultrasonic bath with isopropanol for 7 min. After drying with N_2 , the glass substrates were

treated in a Harrick Plasma Expanded Plasma Cleaner System for another 7 min for further cleaning. The Ag NWs were spun at 2000 rpm for 60 s. This deposition procedure was repeated 10 times to obtain a conductive and transparent film and then the substrate was annealed at 150 °C for 15 min. ZnO NPs were spin-coated at 1000 rpm for 30 s onto the resultant substrate and annealed at 150 °C for 20 min. To deposit PSE between the Ag NW electrodes, a gap was opened by mechanically scratching the Ag NW-ZnO film using a surgical blade that had been heated using the tip of a soldering iron prior to scratching. Finally, the semiconducting purified PSE was drop-casted onto this gap and annealed at 60 °C for 15 min. The whole fabrication was carried out under ambient air conditions.

2.6 Optical characterizations

To measure the absorbance spectrum of the synthesized materials, a Thermo Genesys 10S UV-vis spectrophotometer was utilized. The absorption spectrum of PSE was obtained between 200-700 nm wavelengths with an interval of 1 nm. The samples were added to the hexane-filled quartz cuvettes and absorbance data was collected in arbitrary units (a.u.). The absorbance spectra of silver nanowires and zinc oxide nanoparticles were measured between 400-700 nm wavelengths with an interval of 1 nm. The samples were added to the ethanol-filled quartz cuvettes and absorbance data was collected in arbitrary units (a.u.). The photoluminescence (PL) spectrum of PSE was measured by Agilent-Cary Eclipse fluorescence spectrophotometer 400-700 nm range with an interval of 1 nm wavelengths. The samples were added to the hexane-filled quartz cuvettes, and photoluminescence intensity data was collected in arbitrary units (a.u.).

2.7 Structural characterizations

The surface morphology of the silver nanowires (Ag NW)-zinc oxide nanoparticles (ZnO NP) films was imaged by Zeiss Gemini scanning electron microscope (SEM) and Zeiss Axiocam 506 color optical microscope. Obtained images were characterized using Image J program. The thickness of the films was measured by using a Bruker Dektak XT stylus profilometer. Fourier transform infrared (FT-IR) spectroscopy analyses of pumpkin seed extract was measured by Thermo Scientific Nicolet 6700 FT-IR Spectroscopy.

2.8 Electrical characterizations

Electrical conductivity of the Ag NW-ZnO NP films was determined by measuring sheet resistance of these Ag NW-ZnO NP films, using a handmade four-point probe. For each sample, the average sheet resistance value was determined by measuring five different points. Current-voltage (I-V) measurements were taken using a Keithley 2400 source meter illuminated by hand-held lasers with different wavelengths and monitored the current by using a software. The photocurrent (I_{ph}) is determined by subtracting the dark current (I_{dark}) from the total measured current (I_{total}). The equation used is: $I_{ph}=I_{total}-I_{dark}$ where I_{total} is the current measured when the photodetector is illuminated, and I_{dark} is the current measured in the absence of light. The responsivity of the fabricated photodetectors was measured by the responsivity measurement setup (Keithley 2400 source meter) irradiated by a monochromator-equipped broadband light source was used to measure current-voltage and responsivity of fabricated photodetectors. While measuring the photocurrent under irradiation at various wavelengths between 400 and 650 nm, which are generated with the help of a white light source and a monochromator, a bias voltage is applied to the photodetector.

3. Results and Discussion

Fabrication of optoelectronic devices following simplified processes and employing environmentally friendly materials can lead to a more sustainable and cost-effective technology. Within this framework, pumpkin seeds have a great potential for use in optoelectronics owing to the semiconducting character of their extracts.

In this regard, here we present a new device employing the extracts of *Cucurbita pepo* L. seeds as the active material in a fully solution-processed, transparent metal-semiconductor-metal photodetector architecture. We first prepared the extracts of the pumpkin seeds in hexane with continuous stirring at 60 °C under argon reflux. Following the cleaning procedure, we obtained a clear and greenish oily liquid under daylight and a red-emitting liquid under ultraviolet (UV) light (**Figure 1a**). The concentration of the final material turned out to be 182 mg/mL. We conducted absorbance and photoluminescence measurements to characterize the optical features of pumpkin seed extracts (PSE). PSE absorbs light at a broad range of wavelengths between 200-650 nm and emits a red light under UV excitation, mainly due to the presence of riboflavin and protochlorophylls in pumpkin seeds (Borthakur and Barua, 2014) [7]. As observed in Figure 1a, PSE has a strong absorption peak between 250-300 nm and much weaker absorption bands around 410-450 nm and 550-650 nm. When excited at a wavelength of 420 nm, PSE possesses a weak, broad blue emission in addition to strong emission peaks at ~650 and ~730 nm (**Figure 1b**). We measured the fluorescence quantum yield of the extract as 21%. Following optical characterizations, we conducted FT-IR measurements within a range of 4000-500 cm^{-1} to identify the chemical groups of the active components found in our extract (**Figure 1c**). Previously, *Berezin and V. V. Nechaev* reported that Pumpkin Seeds primarily contain triacylglycerols, along with phenolics and tocopherol in trace amounts [25]. Similar to that study,

our analysis confirmed the presence of hydroxyl groups (O-H) between $3450\text{-}3250\text{ cm}^{-1}$, likely originating from carbohydrates or other bioactive compounds such as carboxyl acids and ketones. We also observed a peak around $3120\text{-}3030\text{ cm}^{-1}$ representing the presence of N-H groups found in amide compounds, as well as the bands at $1105\text{-}1010\text{ cm}^{-1}$ corresponding to lipids, and $2950\text{-}2850\text{ cm}^{-1}$ corresponding to C-H vibrations. Finally, the vibrations around 1450 cm^{-1} suggest the anti-symmetric deformation of CH_3 and CH_2 groups [26].

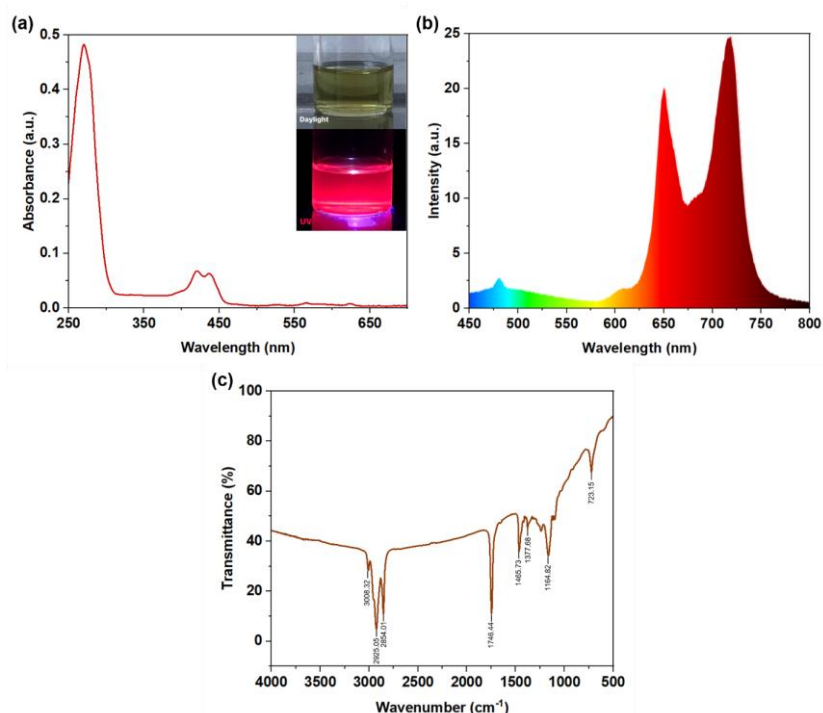


Figure 1. (a) The absorbance spectrum of the PSE. Inset pictures show the photos of the PSE under daylight (above), where the extract reveals a light green color, and under excitation with ultraviolet light (bottom), where the extract has a red emission. (b) The photoluminescence spectrum of the PSE when excited at 420 nm. (c) FT-IR transmittance spectrum of PSE.

Following the optical characterizations of PSE, we carried out the fabrication of an environmentally friendly and cost-effective photodetector. Initially, we implemented the techniques described in our previous publications [17], [18] for the electrode preparation process. Instead of conventional methods involving metal evaporation and lithography, we preferred employing silver nanowires (Ag NW) and zinc oxide nanoparticles (ZnO NP). The silver nanowires synthesized following the procedures reported in Reference [22] exhibited absorption maxima at 350 and 380 nm, corresponding to the longitudinal and transverse modes of plasmon peaks, respectively (**Figure S1**). These findings align with the observations reported by Meenakshi *et al.* [22], [27], [28]. The synthesized Ag NWs were characterized by using scanning electron microscopy (SEM) and Image J software. The SEM images revealed that the Ag NWs possess an average length exceeding $5\ \mu\text{m} \pm 1.08\ \mu\text{m}$ (**Figure S2 (a)**) and an average diameter of approximately $42\ \text{nm} \pm 4.46\ \text{nm}$ (**Figure S2 (b)**).

Since ZnO NPs were found to enhance the stability and conductivity of the films of silver nanostructures [29], we synthesized ZnO NPs using the recipe adapted from Jin *et al.* [23] The absorbance spectrum presented in **Figure S3** indicated a peak at a wavelength of 350 nm, which can be attributed to the intrinsic band-gap absorption of zinc oxides [30], [31], [32]. Subsequently, Dynamic light scattering (DLS) measurements were performed on the ZnO NPs to investigate structural properties of the ZnO nanoparticles (NPs), and the results indicated a particle size of 12 nm. This observation suggests that the NPs possess the potential to occupy the gaps existing between the nanowires, thereby leading to an improvement in conductivity. Supplementary information, **Figure S4**, provides a visual representation of this phenomenon.

To fabricate the proof-of-concept device, we spin-coated Ag NW (10 layers) onto a pre-cleaned glass substrate and annealed it (**Figure 2a**). Afterwards, we spin-coated zinc oxide nanoparticles (ZnO NP) on top of the Ag NW films (**Figure 2b**) to increase the electrical conductivity, transparency and adhesion of the film [17], [33]. To investigate how the number of Ag NW layers affects transparency, we performed multiple spin-coating cycles of the Ag NW solution, followed by five spin-coating cycles of the ZnO NP dispersion. As depicted in **Figure S5**, the transmittance of the Ag NW-ZnO NP films decreases as the number of spin-coating cycles increases. However, even after two spin-coating cycles, the transmittance remains above 90%. Even after ten spin-coating cycles, the transmittance is still higher than 85% in the spectral range over 580 nm. In comparison, commercially available indium tin oxide

films (ITO) have transmittances of around 90% in the visible range [34]. These results indicate that the levels of transparency we achieved are similar to what has been reported in the literature [35]. Afterward, we examined the sheet resistance of the 10 layers of Ag NW-coated film. Characterizations conducted by a four-probe measurement set-up demonstrated that the sheet resistance of the Ag NW/ZnO NP transparent film is 154 ohms/square. When we compare this sheet resistance with commercially available ITO, we realized that with the same thickness of 165 nm, our conductive film has slightly higher sheet resistance (154 ohms/square) than ITO (60-90 ohms/square) [36], [37], [38], [39]. Therefore, this result shows that the levels of sheet resistance we obtained are comparable with the transparent conductive films in the literature. Then, we scratched this layer with a surgical blade and drop-casted the semiconductive plant-based solution into the resulting gap as the active layer (**Figure 2c**). Subsequently, we annealed the device at 60 °C for 15 min. The actual image of our photodetector is shown in **Figure 2d**. To examine potential chemical alterations in the Pumpkin Seed extract following thermal treatment at 60°C, we conducted FTIR analysis. The results indicated no significant changes in the structure of the PSE concerning the locations of vibrations (**Figure S6**).

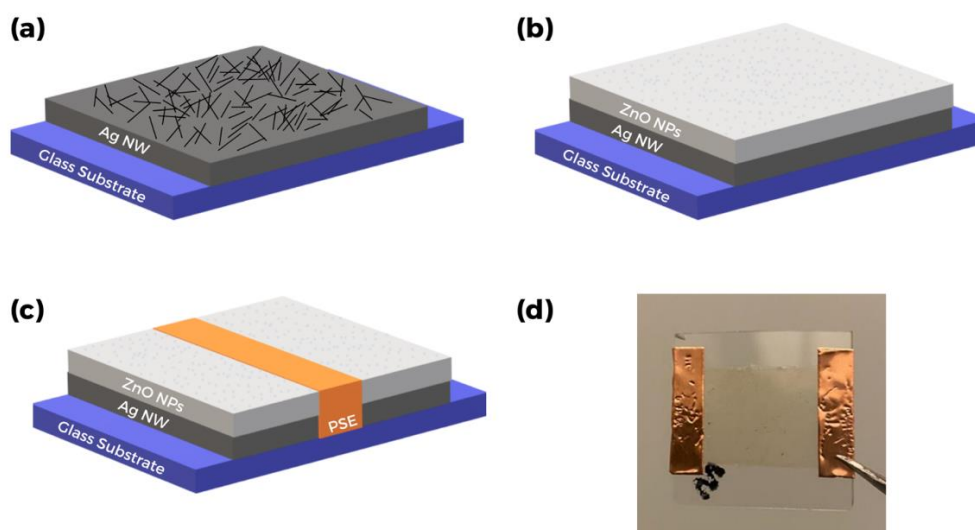


Figure 2. (a-c) Schematic representation of the metal-semiconductor-metal PSE photodetector fabrication procedure. (d) Photograph of the fabricated device.

The structure of the scratched surface prior to PSE deposition was characterized using both optical microscopy and SEM (Figure 3). Results reveal the width of the gap as $\sim 30\ \mu\text{m}$, which is wider than the typical gaps opened using lithography but narrow enough to observe variations in the resistance upon exposure to light [17], [18]. Profilometer measurements indicate the thickness of Ag NW-ZnO NP film to be $\sim 165\ \text{nm}$; the film thickness was measured as $\sim 22\ \mu\text{m}$ after drop-casting PSE on top of the Ag NW and ZnO coated film (**Figure S7**).

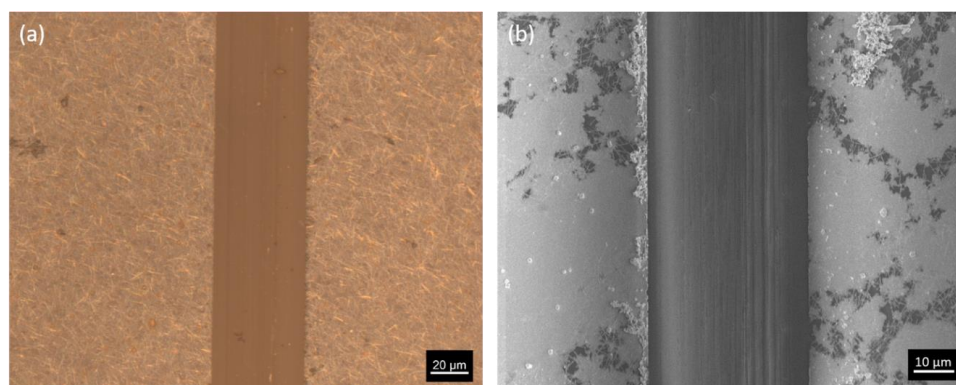


Figure 3. (a) Optical microscope and (b) SEM images of Ag NW-ZnO NP electrodes after scratching with a surgical blade.

After the fabrication of the photodetectors (PDs), optoelectronic characterizations were conducted to quantitatively assess their performance. For this aim, photocurrent measurements were performed on the

fabricated PDs by exciting the pumpkin seed extract (PSE) at different wavelengths and bias voltages. Additionally, responsivity calculations were carried out, which is a metric that characterizes the ability of the photodetector to convert light into electricity and calculated according to Equation 1 [40] where I_{ph} and P_o stand for the photocurrent and incident optical power, respectively [41].

$$R_{\lambda} = \frac{I_{ph}}{P_o} \quad (\text{A/W}) \quad (1)$$

As shown in **Figure 4a**, the applied bias and wavelength of the incident light significantly affect the responsivity of the fabricated photodetectors. The maximum responsivity recorded was measured as ~ 1.61 mA/W at 5 V bias voltage under 620 nm light exposure. With increasing voltage, the stronger electric field between the electrodes makes it simpler to collect charges which enhances the photocurrent and responsivity. On the hand, the recorded, relatively low responsivity can be attributed to the PSE extract that did not fully dry due to the oily nature of the extract even after treating it at 60 °C. When we compare this wavelength dependence with the absorbance of the PSE, we observe that the responsivity decreases at shorter wavelengths, whereas the absorbance of PSE increases. This demonstrates that the contacts cannot collect the generated electron-hole pairs as effectively as the ones generated at longer wavelength exposures. We attribute the observed difference to the thickness of the PSE layer, which is approximately 22 micrometers due to the drop-casting method, in combination with the not fully-dried film causing exciton formation far away from the contacts upon excitation with short-wavelength photons. Since the PSE absorbs light at shorter wavelengths stronger than light at longer wavelengths, light at shorter wavelengths has a substantially smaller penetration depth. Therefore, the highly energetic photons are only absorbed in the first few microns of the top portion of the device and are unable to reach the active region to be harvested, reducing the responsivity of the photodetector. When these results are compared with the quantum dot-based photodetectors and organic photodetectors, still our plant-based photodetector needs improvement in their responsivities. This performance difference results from the broader absorption spectra that QDs have, making them more efficient at absorbing specific wavelengths of light. Quantum dots also tend to exhibit a higher quantum efficiency, representing the proportion of absorbed photons that contribute to photocurrent by generating charge carriers.

When these results are compared with the quantum dot-based photodetectors and organic photodetectors [42], [43], [44], [45], [46], our plant-based photodetector still requires enhancement in its responsivity. Quantum dot-based photodetectors typically exhibit responsivities in the range of 0.1 to 1 A/W, with some advanced devices reaching up to 109 A/W depending on the specific material and device architecture [47]. Organic photodetectors, on the other hand, usually show responsivities between 0.1 and 0.5 A/W [48]. In comparison, our plant-based photodetector currently demonstrates a responsivity of ~ 1.61 mA/W at 5 V bias voltage under 620 nm light exposure. While this is lower than the typical values for QD and organic photodetectors, it is important to note that this is a preliminary result, and there is significant potential for improvement through further optimization of the device structure and material properties. This performance disparity is attributed to the broader absorption spectrum inherent to quantum dots, which enables them to absorb specific wavelengths of light more efficiently. Additionally, quantum dots tend to demonstrate higher quantum efficiency, reflecting a greater proportion of absorbed photons contributing to photocurrent by generating charge carriers [49], [50]. As a result, quantum dot photodetectors generally offer superior responsivity compared to their organic counterparts.

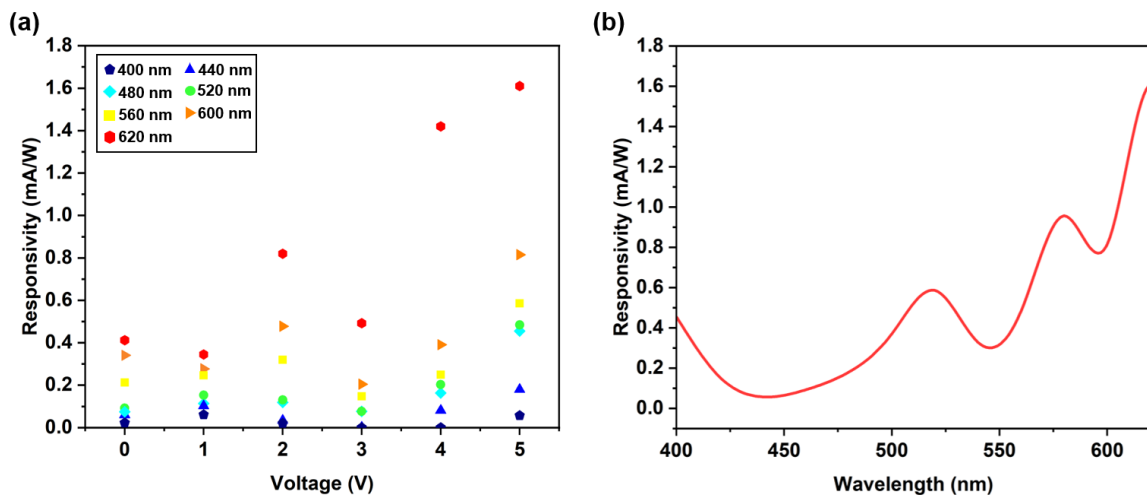


Figure 4. (a) The responsivity of the PSE photodetectors at different bias voltages in the range of 400-620 nm. (b) The responsivity spectrum of PSE photodetectors at a bias voltage of 5 V as a function of wavelength.

4. Discussion and Conclusion

Here, we introduced semiconducting plant extracts as a sustainable alternative to conventional semiconductor materials for optoelectronic applications. In particular, we demonstrated the potential of plant extracts in metal-semiconductor-metal photodetectors using the extract of *Cucurbita pepo L.* (pumpkin) seeds. To further elaborate the environmental-friendliness, we employed solution-processed electric contacts made of Ag nanowires and ZnO nanoparticles patterned using a surgical blade instead of lithography. The resulting conductive films exhibited a sheet resistance <100 ohms/square while keeping the optical transparency above 85%. By simply drop-casting the extract between the electrodes, we completed the photodetector structure. To the best of our knowledge, our device is the first active optoelectronic device made of plant extracts. Our proof-of-concept device exhibited responsivities up to 1.61 mA/W. Through thickness, material, and device architecture optimizations, the performance of the device can be further enhanced such that it can compete with the materials used ubiquitously in literature. We believe that our results potentially form the building blocks for realizing a more sustainable and cost-effective material system to be employed in active optoelectronic devices.

Acknowledgment

ZSE acknowledges to The Scientific and Technological Research Council of Türkiye (TUBİTAK) ARDEB 1001 Grant No:123M876. TE acknowledges the BAGEP Award from the Science Academy and the GEBIP Award from the Turkish Academy of Sciences (TÜBA).

References

- [1] Proestos, C., & Varzakas, T. 2017. Aromatic Plants: Antioxidant Capacity and Polyphenol Characterisation. *Foods*, 6(4), 1–7.
- [2] Demmig-Adams, B., Gilmore, A. M., & W. W. A. Iii. 1996. Carotenoids 3: in vivo function of carotenoids in higher plants. *FASEB J*, 10(4), 403–412.
- [3] Langi, P., Kiokias, S., Varzakas, T., & Proestos, C. 2018. Carotenoids: From Plants to Food and Feed Industries. *Methods in Molecular Biology*, 1852, 57–71.
- [4] Proestos, C. 2020. The Benefits of Plant Extracts for Human Health. *Foods*, 9(11), 1653.
- [5] Croce, A. C., & Bottiroli, G. 2014. Autofluorescence spectroscopy and imaging: A tool for biomedical research and diagnosis. *European Journal of Histochemistry*, 58(4), 320–337.
- [6] Donaldson, L. 2020. Autofluorescence in plants. *Molecules*, 25(10).
- [7] Borthakur, P. R., & Barua, A. G. 2014. Fluorescence studies of the seeds of the pumpkin (*Cucurbita pepo L.*). *National Academy Science Letters*, 37(3), 275–279.
- [8] Nawirska-Olszańska, A., Kita, A., Biesiada, A., Sokół-Łętowska, A., & Kucharska, A. Z. 2013. Characteristics of antioxidant activity and composition of pumpkin seed oils in 12 cultivars. *Food Chemistry*, 139(1–4), 155–161
- [9] Šamec, D., et al. 2022. The potential of pumpkin seed oil as a functional food-A comprehensive review of chemical composition, health benefits, and safety. *Comprehensive Reviews in Food Science and Food Safety*, 21(5), 4422–4446.
- [10] Liu, Y., Lininger, A. S., McCaskey, L. N., & Thomas, R. M. 2023. Separation of fluorescent protochlorophyllide from green pumpkin seed using column chromatography. *Journal of Chemical Education*, 100(1), 312–315.
- [11] Barberini, L., Cadeddu, S., Giannattasio, A., & Lai, A. 2002. Gallium arsenide photodetectors for imaging in the far ultraviolet region. *Applied Physics Letters*.

- [12] Song, J., et al. 2021. High-efficiency and high-speed germanium photodetector enabled by multiresonant photonic crystal. *Nanophotonics*, 10(3), 1081–1087.
- [13] Dou, L., et al. 2014. Solution-processed hybrid perovskite photodetectors with high detectivity. *Nature Communications*, 5(1), 1–6.
- [14] Biondi, M., et al. 2021. Facet-Oriented Coupling Enables Fast and Sensitive Colloidal Quantum Dot Photodetectors. *Advanced Materials*, 33(33), 2101056.
- [15] Chow, P. C. Y., Someya, T., Chow, P. C. Y., & Someya, T. 2020. Organic Photodetectors for Next-Generation Wearable Electronics. *Advanced Materials*, 32(15), 1902045.
- [16] Wu, Z., Zhai, Y., Kim, H., Azoulay, J. D., & Ng, T. N. 2018. Emerging Design and Characterization Guidelines for Polymer-Based Infrared Photodetectors. *Accounts of Chemical Research*, 51(12), 3144–3153.
- [17] Savas, M., Yazici, A. F., Arslan, A., Mutlugün, E., & Erdem, T. 2023. Toward sustainable optoelectronics: solution-processed quantum dot photodetector fabrication using a surgical blade. *Optics Express*, 62(2), 027102.
- [18] Savas, M., Yazici, A. F., Arslan, A., Mutlugün, E., & Erdem, T. 2022. Simple, sustainable fabrication of fully solution-processed, transparent, metal-semiconductor-metal photodetectors using a surgical blade as an alternative to conventional tools. *Proceedings of SPIE*, 12131, 181–193.
- [19] Das, N., Karar, A., Vasiliev, M., Tan, C. L., Alameh, K., & Lee, Y. T. 2011. Analysis of nano-grating-assisted light absorption enhancement in metal–semiconductor–metal photodetectors patterned using focused ion-beam lithography. *Optics Communications*, 284(6), 1694–1700.
- [20] Qin, L., Shing, C., & Sawyer, S. 2011. Metal semiconductor metal ultraviolet photodetectors based on zinc-oxide colloidal nanoparticles. *IEEE Electron Device Letters*, 32(1), 51–53.
- [21] Chou, S. Y. 1999. Nanoscale GaAs metal-semiconductor-metal photodetectors fabricated using nanoimprint lithography. *Applied Physics Letters*.
- [22] Kim, T., Canlier, A., Kim, G. H., Choi, J., Park, M., & Han, S. M. 2013. Electrostatic spray deposition of highly transparent silver nanowire electrode on flexible substrate. *ACS Applied Materials & Interfaces*, 5(3), 788–794.
- [23] Jin, X., et al. 2018. Bright alloy type-II quantum dots and their application to light-emitting diodes. *Journal of Colloid and Interface Science*, 510, 376–383.
- [24] Alexandrov, A., [et al.]. 2020. Al-, Ga-, Mg-, or Li-doped zinc oxide nanoparticles as electron transport layers for quantum dot light-emitting diodes. *Scientific Reports*, 10(1), 1–11.
- [25] Berezin, K. V., & Nechaev, V. V. 2005. Calculation of the IR spectrum and the molecular structure of β -carotene. *Journal of Applied Spectroscopy*, 72(2), 164–171.
- [26] Schlücker, S., Szeghalmi, A., Schmitt, M., Popp, J., & Kiefer, W. 2003. Density functional and vibrational spectroscopic analysis of β -carotene. *Journal of Raman Spectroscopy*, 34(6), 413–419.
- [27] Ghorbani, M. M., & Taherian, R. 2018. Methods of measuring electrical properties of material. In *Electrical Conductivity in Polymer-Based Composites: Experiments, Modelling, and Applications*, 365–394.
- [28] Meenakshi, P., Karthick, R., Selvaraj, M., & Ramu, S. 2014. Investigations on reduced graphene oxide film embedded with silver nanowire as a transparent conducting electrode. *Solar Energy Materials and Solar Cells*, 128, 264–269.
- [29] Tang, Y., et al. 2018. Low-temperature solution processed flexible silver nanowires/ZnO composite electrode with enhanced performance and stability. *Journal of Alloys and Compounds*, 747, 659–665.

- [30] Khorsand Zak, A., Razali, R., Abd Majid, W. H., & Darroudi, M. 2011. Synthesis and characterization of a narrow size distribution of zinc oxide nanoparticles. *International Journal of Nanomedicine*, 6(1), 1399–1403.
- [31] Singh, D. K., Pandey, D. K., Yadav, R. R., & Singh, D. 2012. A study of nanosized zinc oxide and its nanofluid. *Pramana - Journal of Physics*, 78(5), 759–766.
- [32] Aldalbahi, A., et al. 2020. Greener synthesis of zinc oxide nanoparticles: Characterization and multifaceted applications. *Molecules*, 25(18).
- [33] Alam, F., & Balani, K. 2017. Role of silver/zinc oxide in affecting de-adhesion strength of *Staphylococcus aureus* on polymer biocomposites. *Materials Science and Engineering C: Materials for Biological Applications*, 75, 1106–1114.
- [34] Zhang, J., Chia, A. C. E., & Lapierre, R. R. 2014. Low resistance indium tin oxide contact to n-GaAs nanowires. *Semiconductor Science and Technology*, 29(5), 054002.
- [35] Ahmed, N. M., Sabah, F. A., Abdulgafour, H. I., Alsadig, A., Sulieman, A., & Alkhoaryef, M. 2019. The effect of post annealing temperature on grain size of indium-tin-oxide for optical and electrical properties improvement. *Results in Physics*, 13.
- [36] Kang, S. W., Lee, H. J., Cho, S. H., Cheong, W. S., Lee, G. H., & Song, P. K. 2012. Effects of Sn concentration on ultrathin ITO films deposited using DC magnetron sputtering. *Journal of Nanoelectronics and Optoelectronics*, 7(5), 494–497.
- [37] Kitova, S., Mankov, V., Dimov, D., Strijkova, V., Malinowski, N. 2021. High quality ITO thin films for application as conductive transparent electrodes." *Bulgarian Chemical Communications* 48, 196–201.
- [38] Hussain, S. Q., et al. 2014. RF magnetron sputtered ITO:Zr thin films for the high efficiency a-Si:H/c-Si heterojunction solar cells. *Metals and Materials International*, 20(3), 565–569.
- [39] Mazur, M., Kaczmarek, D., Domaradzki, J., Wojcieszak, D., Song, S., & Placido, F. 2010. Influence of thickness on transparency and sheet resistance of ITO thin films. In *The Eighth International Conference on Advanced Semiconductor Devices and Microsystems*, 65–68.
- [40] Xu, K., Zhou, W., Ning, Z., Xu, K., Zhou, W., & Ning, Z. 2020. Integrated structure and device engineering for high performance and scalable quantum dot infrared photodetectors. *Small*, 16(47), 2003397.
- [41] Hui, R., & O'Sullivan, M. 2009. *Fiber Optic Measurement Techniques*. Fiber Optic Measurement Techniques.
- [42] Pu, K., et al. 2023. A flexible sensitive visible-NIR organic photodetector with high durability. *Advanced Materials Technologies*, 8(16), 2300207.
- [43] Kielar, M., Dhez, O., Pecastaings, G., Curutchet, A., & Hirsch, L. 2016. Long-term stable organic photodetectors with ultra-low dark currents for high detectivity applications. *Scientific Reports*, 6(1), 1–11.
- [44] Dang, Q., et al. 2023. Enhanced gain in organic photodetectors using the polymer with singlet open-shell ground state. *Angewandte Chemie*, e202312538.
- [45] Liu, Q., et al. 2019. Hybrid Graphene/Cu₂O Quantum Dot Photodetectors with Ultrahigh Responsivity. *Advanced Optical Materials*, 7(20), 1900455.
- [46] Wu, X., Zhao, B., Zhang, J., Xu, H., Xu, K., & Chen, G. 2019. Photoluminescence and Photodetecting Properties of the Hydrothermally Synthesized Nitrogen-Doped Carbon Quantum Dots. *Journal of Physical Chemistry C*, 123(42), 25570–25578.
- [47] Kwak, D. H., Ramasamy, P., Lee, Y. S., Jeong, M. H., Lee, J. S. 2019. High-Performance Hybrid InP QDs/Black Phosphorus Photodetector. *ACS Appl. Mater. Interfaces*, 11(32), 29041–29046.

- [48] Ren, H., Chen, J. D., Li, Y. Q., Tang, J. X. 2021. Recent Progress in Organic Photodetectors and their Applications. *Advanced Science*, 8(1).
- [49] Hu, L., [et al.]. 2014. Multifunctional carbon dots with high quantum yield for imaging and gene delivery. *Carbon N Y*, 67, 508–513.
- [50] Nasilowski, M., [et al.]. 2015. Gradient CdSe/CdS Quantum Dots with Room Temperature Biexciton Unity Quantum Yield. *Nano Lett*, 15(6), 3953–3958.